ACS APPLIED POLYMER MATERIALS

pubs.acs.org/acsapm Article

Revealing the Molar Mass Dependence on Thermal, Microstructural, and Electrical Properties of Direct Arylation Polycondensation Prepared Poly(3-hexylthiophene)

Qingchun Qi, Yuan Zhong, Yang Liu, Mengyuan Gao, Zhongxiang Peng, Saimeng Li, Wenchao Zhao, Huizhen Ke,* Jidong Zhang, and Long Ye*

Cite This: ACS Appl. Polym. Mater. 2022, 4, 1826−1835 Read Online

ACCESS | Metrics & More | Article Recommendations | Supporting Information

ABSTRACT: Poly(3-hexylthiophene) (P3HT) is a "fruit fly" conjugated polymer in the field of organic electronics due to its simple chemical structure, decent photoelectric properties, and low cost. To date, the design of nonfullerene acceptors matching P3HT and the synthesis of high-quality P3HT via sustainable methods hold tremendous promises for advancing the P3HT solar cells. The use of P3HT via direct arylation polycondensation (DArP) has recently proven to be an efficient means for constructing efficient polythiophene solar cells, while the intrinsic properties of DArP prepared P3HT remain poorly understood, thus impeding further performance enhancements. Herein, six batches of P3HTs with weight-average molecular weights from 8.5 to 73.9 kg/mol were successfully synthesized via DArP, and multitechnique characterizations were employed to investigate the molecular weight effect of P3HT on its optical properties, crystallization behaviors, morphology, and electrical properties. P-52k with relatively high crystallinity and hole mobility was applied in photovoltaic devices matching a variant of the popular nonfullerene acceptor Y6. This photovoltaic combination afforded a good power conversion efficiency of over 7% in P3HT/nonfullerene solar cells. Importantly, this research not only provides insights into the physical properties of DArP prepared P3HT as a function of molecular weight but reveals the correlation between the key structure parameter and the electrical performance of P3HT for optoelectronic applications as well.

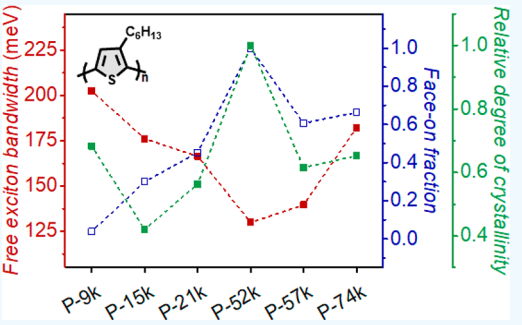

KEYWORDS: *P3HT, molecular weight, direct arylation polycondensation, thermal properties, nonfullerene solar cells*

1. INTRODUCTION

Polythiophenes are often referred to as the "fruit fly"[1] of organic semiconducting polymers because of their straightforward synthesis, high charge transport mobility, and mass production capacity and, therefore, are expected to become promising candidates for electronic devices including field-effect transistors,[2−5] photodetectors,[6] light-emitting diodes,[7−10] and organic photovoltaics[11−15] in particular. In addition to the molecular structure characteristics such as backbone configuration and the length, branching, and polarity of the side chains, the intrinsic properties of polythiophenes are also affected by other factors. For example, molecular weight, as a critical structure parameter, plays an important role in the control of optical properties, crystallization behaviors, solid-state stacking, and electronic performances of polythiophenes.[16−21] Paquin et al.,[22] for instance, observed that the balanced intramolecular and intermolecular exciton coupling could result in the long exciton coherence length, which was responsible for the more planar conformation of high-molecular-weight poly(3-hexylthiophene) (P3HT). Kline and co-workers[23] systematically investigated the morphology and crystallization behavior of P3HT with different molecular weights by atomic force microscopy (AFM) and X-ray diffraction (XRD) to establish the relationship between molecular weight and charge carrier mobility. Though P3HT with low molecular weights obtained a relatively high degree of crystallinity, they generally possessed lower mobility due to the domain boundaries and the shorter chains. Liu et al.[20] found that the crystallinity of P3HT reached the maximum for intermediate molecular weight at which the best photovoltaic performance could be achieved in fullerene-based devices. Besides the above studies, many more efforts have been devoted to the research of P3HT to further deepen the understanding of the mechanisms of organic photovoltaic devices.

Received: November 19, 2021
Accepted: February 7, 2022
Published: February 21, 2022

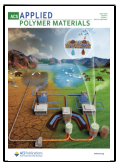

https://doi.org/10.1021/acsapm.1c01651
ACS Appl. Polym. Mater. 2022, 4, 1826−1835

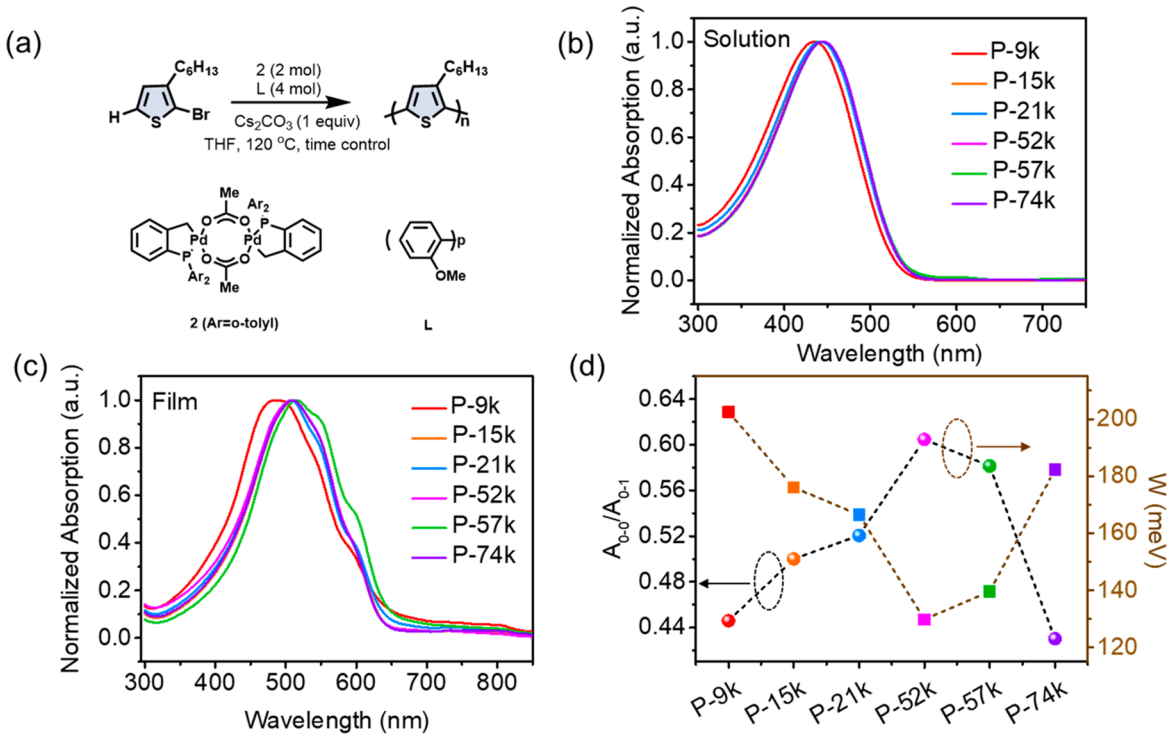

Figure 1. (a) Synthetic route of P3HT with different weight-average molecular weights prepared by DArP. Normalized UV−vis absorption spectra of P3HTs with different molecular weights in (b) solution and (c) the solid state. (d) The plot of the ratios of A_{0-0} and A_{0-1} and the free exciton bandwidths of P3HTs.

So far, the P3HTs used in most of the studies were synthesized by conventional synthetic methods[24] such as Kumada, Negishi, Stille, and Suzuki polymerization. Among these, the polymerization to regioregular P3HT based on nickel-catalyzed Kumada cross-coupling was first developed by McCullough and Lowe.[25] Nevertheless, these conventional synthetic routes are often accompanied by various disadvantages including multistep procedures and expensive purification as well as environmental pollution.[26] Direct arylation polycondensation (DArP), overcoming the drawbacks of traditional cross-coupling reactions, was transferred from small molecule coupling into polymer synthesis by Lemaire and co-workers[27] in 1999 for the first time. The regioregularity of the obtained poly[3-(3-methyl-pentyl)thiophene] could reach up to ∼90%, while the molecular weight of the resulting product was lower than 3 kg/mol. In 2010, Ozawa and co-workers[28] developed a regioregular P3HT with a number-average molecular weight higher than 30 kg/mol by selecting a highly efficient Herrmann's catalyst for DArP of 2-bromo-3-hexylthiophene, and the yield of this reaction was as high as 99%. In addition, DArP is an eco-friendly and atomic economy method for the synthesis of these conjugated polymers.[29] The production cost of P3HT made by DArP is estimated to be <10 $/g, which is significantly cheaper than the commercially accessed ones.[30] Some research groups in the community have recently shifted to the use of DArP prepared P3HT in solar cells. For instance, Liu and co-workers[30,31] have successfully demonstrated the great potential of DArP to prepare P3HT and its analogues for nonfullerene solar cells. In certain cases, the DArP prepared P3HT can even outperform conventionally synthesized P3HT in organic solar cells when an identical nonfullerene acceptor is used.[30] The photovoltaic performance of P3HT prepared via DArP has been well explored, while the optical properties, thermal behaviors, crystalline structure, and electrical performances of the DArP prepared P3HT remain poorly exploited, which impede the further advance of these critically important and eco-friendly made polythiophenes.

In this work, six batches of P3HT with molecular weights in the range of 8.5−73.9 kg/mol (in the form of weight-average) were successfully prepared via DArP, and a full set of characterization techniques including ultraviolet−visible (UV−vis) absorption spectroscopy, differential scanning calorimetry (DSC), dynamic mechanical analysis (DMA), grazing incidence wide-angle X-ray scattering (GIWAXS), atomic force microscopy (AFM), and transmission electron microscopy (TEM) were performed to investigate the intrinsic properties of these P3HT materials. According to the UV−vis absorption spectra, the conjugation length of P3HT reached the maximum for the intermediate molecular weight. The thermal analysis illustrated that the glass transition temperature (T_g) showcases an obvious increase at 52 kg/mol. The microscopic results demonstrated that low-molecular-weight P3HTs were more likely to crystallize and form the isolated grain boundaries, while P3HT with a molecular weight higher than 9 kg/mol generally possessed the uniform morphology. Moreover, with the increase of molecular weight, the DArP prepared P3HT transformed from an edge-on stacking manner to a face-on dominated packing orientation, and the intensity of the (010) diffraction pattern along the out-of-plane direction reached the maximum at 52 kg/mol exhibited by GIWAXS. Consequently, the DArP prepared P3HT with a moderate molecular weight of ∼50 kg/mol achieved the highest hole mobility in single charge-carrier diodes, and the corresponding photovoltaic devices employing a recently emerged nonfullerene small molecule acceptor surpassed 7%

https://doi.org/10.1021/acsapm.1c01651
ACS Appl. Polym. Mater. 2022, 4, 1826−1835

Table 1. Basic Molecular Weight Information and Some Physical Properties of P3HT

P3HT batch	M_n (kg/mol)	M_w (kg/mol)	PDI	T_m (°C)	T_c (°C)	ΔH_m (J/g)	T_g (°C)
P-9k	5.3	8.5	1.59	136.6	111.8	3.6	22.1
P-15k	10.9	15.2	1.40	198.9	169.2	10.5	15.4
P-21k	12.8	21.1	1.64	190.4	163.5	10.9	15.4
P-52k	28.5	52.3	1.84	176.1	139.6	8.8	18.5
P-57k	29.3	57.1	1.95	191.0	150.7	7.3	15.7
P-74k	29.3	73.9	2.52	202.3	164.2	8.9	23.7

efficiency, highlighting the bright future of these eco-friendly made and scalable polythiophene materials.

2. RESULTS AND DISCUSSION

2.1. Materials Synthesis. A series of P3HTs with different molecular weights were synthesized by tuning the reaction time of DArP, and the synthetic route was shown in Figure 1a. Figure S1 shows the ^{1}H NMR spectra of the obtained polymers recorded on a Bruker AVANCE III spectrometer in chloroform-d ($CDCl_3$). The regioregularity of the P3HT samples was calculated via the peak integration of the α-methylene signals of the 3-hexyl groups at δ 2.81 (HT) and 2.59 (HH). All batches of P3HTs share a similar regioregularity of ∼90%, except for the lowest and the highest molecular weight ones, whose regioregularities are 84% and 87%, respectively. The average molecular weight and polydispersity summarized in Table 1 were obtained by the gel permeation chromatography (GPC) in tetrahydrofuran (THF) at room temperature. P-74k, showing a comparable number-average molecular weight to P-57k but a different polydispersity index (PDI), was used for a comparison to P-57k. The polydispersity indices of P-57k and P-74k are 1.95 and 2.52, respectively. ZY-4Cl was synthesized by our laboratory according to the procedures reported earlier.[32]

2.2. Optical Properties. Ultraviolet−visible (UV−vis) absorption spectra were used to reveal the molecular aggregation of P3HTs. The solution absorption spectra of P3HTs with molecular weights higher than 9 kg/mol exhibit similar shapes. As shown in Figure 1b, there is only one broad absorption peak and the maximum absorption at ∼445 nm does not change substantially with the increase of molecular weight. Compared with the maximum absorption of higher molecular weight ones (M_w > 15 kg/mol), P-9k, however, has a slight blueshift, which is mainly due to the relatively low regioregularity. The differences in the solution absorption spectra of P3HT with different regioregularities have been revealed by a large number of studies according to Adachi et al.[33] and Custódio Mota et al.[34] They pointed out that the absorption peak of regioregular P3HT was in the range of 440−450 nm while the regiorandom P3HT containing HH and TT configurations defects blue-shifted to ∼420 nm. This phenomenon can be attributed to the decreased effective conjugation length resulting from the twisting backbone of regiorandom P3HT.

Compared with the solution absorption spectra, the absorption spectra of P3HT films (Figure S2a) have a redshift above 50 nm, resulting from the enhanced rigidity of the P3HT backbone in the solid state. Besides, all P3HTs exhibit the obvious characteristic peaks at ∼560 and ∼600 nm, and the intensities of these shoulder peaks become stronger with molecular weights increasing from 9 to 57 kg/mol. In contrast to P-57k, the characteristic peaks of P-74k shift to a shorter wavelength region, and the intensities of these peaks decrease slightly. We infer that the decreased degree of order in P-74k is mainly due to the simultaneously increased fractions of shorter and longer polymer chains. In spite of the contribution of the highly ordered shorter polymer chains, P-74k has a poor alignment due to the excessive variability in the distribution of molecular weight. The maximum absorption of low molecular weight P3HT (i.e., P-9k) is at 494 nm, while P3HT with a molecular weight higher than 9 kg/mol displays main peaks at ∼510 nm. As displayed in Figure S2b,c, the maximum absorption coefficients and the shoulder-peak intensities of the P3HT films at ∼560 and ∼600 nm enhance significantly after annealing at 130 °C for 10 min except for those of P-52k. Different from the maximum absorption, the shoulder peaks of P3HT films blue-shift slightly after annealing (Figure 1c), which can be attributed to the thermal-induced continuous transition from a planar rod-like to a twisted coil-like conformation.[35]

Gaussian multipeak fitting was employed to decompose the absorption spectra of annealed P3HT films and localize the individual absorption peak contributing to the optical absorption of P3HT (Figure S3 and Table S1). The peaks at ∼470, ∼510, ∼550, and ∼600 nm correspond to the 0−3, 0−2, 0−1, and 0−0 excitonic peaks, respectively.[36] The intensity of the characteristic peaks at ∼550 and ∼600 nm also can be denoted as A_{0-1} and A_{0-0}, respectively. According to Clark et al.,[37] the ratio of 0−0 and 0−1 peak absorbance is the indicator of interchain coupling energy, related to the free exciton bandwidth W, and can be calculated by the following equation:

$$\frac{A_{0-0}}{A_{0-1}} \approx \frac{n_{0-1}}{n_{0-0}}\left(\frac{1 - 0.24W/E_p}{1 + 0.073W/E_p}\right)^2 \quad (1)$$

where n_{0-i} is the real part of the refractive index at 0−i and E_p is the energy generated by the vibration of the polymer backbone. The values of $\frac{n_{0-1}}{n_{0-0}}$ and E_p are 0.98 and 180 meV, respectively. Therefore, we can get the free exciton bandwidth of P3HT with different molecular weights by substituting the intensity of the characteristic peaks 0−0 and 0−1 into the above formula. According to Clark et al.,[38] the interchain coupling energy estimated by the ratio of A_{0-0} and A_{0-1} is inversely proportional to the conjugation length and intrachain order of P3HT. From Figure 1d and Table S2, the free exciton bandwidth of P3HT decreases from 202.52 meV for P-9k to 129.86 meV for P-52k, which indicates that the conjugation length of P3HT increases with the increase of molecular weight. It can be seen that the smallest free exciton bandwidth is achieved for the intermediate molecular weight P3HT (i.e., P-52k), corresponding to the weakest exciton coupling and the highest crystal quality. The ratio of A_{0-0} and A_{0-1} decreases slightly when the molecular weight of P3HT exceeds 52 kg/mol, which is mainly due to the higher content of the disordered conformation. In summary, P3HTs with a similar

https://doi.org/10.1021/acsapm.1c01651
ACS Appl. Polym. Mater. 2022, 4, 1826−1835

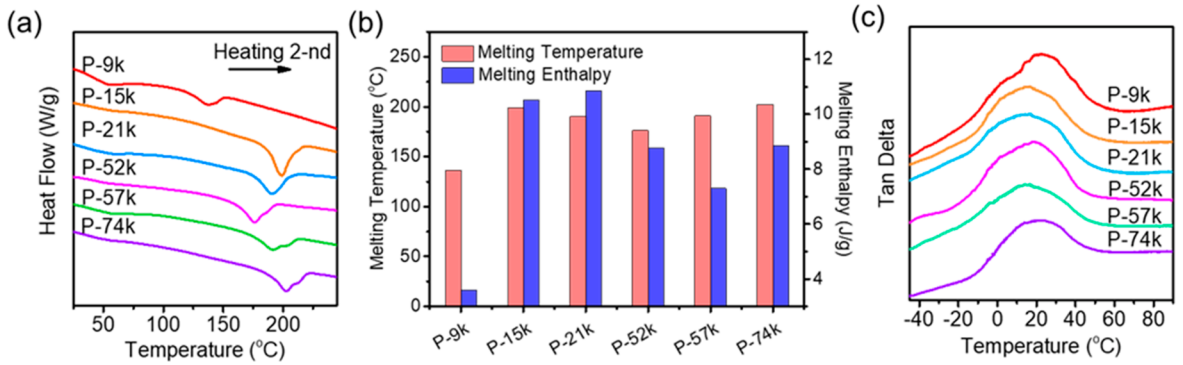

Figure 2. (a) Second-heating DSC curves of different molecular weight P3HTs samples. (b) The melting temperature and melting enthalpy of P3HTs. (c) The tan delta curves of P3HTs measured by DMA.

regioregularity exhibit a similar maximum absorption in THF, while there is a significant blueshift of that of low regioregular P3HT due to the existence of the configuration defect. The maximum absorption of P3HT in the solid state red-shifts gradually with the increase of molecular weight, whereas the location of the individual peak does not change substantially before and after annealing. For P3HT with a higher PDI, the increased lower and higher molecular weight fractions disturb its aggregation and degree of order. The shoulder peaks of P3HTs blue-shift slightly after annealing because of the thermal action, and the intensities of these peaks increase significantly. We also infer that P-52k with the largest conjugation length has the most ordered microstructure in thin films.

2.3. Thermal Properties. We employed DSC and DMA to investigate the thermal properties of the P3HTs of different batches. The melting temperatures and enthalpies of fusion, as well as crystallization temperatures determined by the second heating and first cooling curves, respectively, from the DSC measurement, are summarized in Table 1. With the increase of P3HT molecular weight from 9 to 15 kg/mol, the melting temperature increases from 136.6 to 198.9 °C along with the increasing melting enthalpy (Figure 2a,b), indicating the higher crystalline quality. According to Chang et al.,[39] the chemical defects and impurities in P3HT with low molecular weight are responsible for the decreased melting temperature. Notably, the melting temperature of P3HT with a molecular higher than 21 kg/mol decreases significantly accompanied by the decrease of the melting enthalpy, especially for P-52k. We surmise that the onset of the chain folding resulting from the increased chain length and the enhanced flexibility of the polymer chains at which they transform from the isolated extended conformation to the connected two-dimensional morphology is responsible for the phenomenon, in which less energy is required to melt the crystals. Nevertheless, the value of molecular weight at which chain folding occurs differs significantly in literature reports.[35,40] It seems that the majority of studies hold that the turning point is in the range of 10−15 kg/mol, while Chandrasekaran et al. pointed out that the molecular weight of the onset of chain folding was 88 kg/mol.[41] Chang et al.,[39] nevertheless, found that the mobility of P3HT with molecular weight in the range of 29−52 kg/mol was the highest due to the highest crystalline quality. With the increase of molecular weight from 52 to 74 kg/mol, the melting and crystallization temperatures first increase and then tend to saturate. The increased melting temperature and the decreased melting enthalpy of higher molecular weight P3HT suggest that both the degree of crystallinity and the amorphous content increase with the increase of molecular weight. Compared with P-57k, P-74k obtains the higher melting temperature and enthalpy, which can be attributed to the stronger entanglement in the melting process resulted from the increased longer polymer chain content. It can be observed that there is more than one peak in each endothermic process for P-52k, P-57k, and P-74k; this phenomenon called irreversible (or nonequilibrium) melting can be explained by the chain reorganization and crystal perfection during melting transition.[42] Besides, there is a reversible transition in the range of 50−60 °C, which is mainly due to the side-chain melting.[43]

The DMA measurement was performed to further understand the relaxation and crystallization behavior of P3HTs in different batches (Figure S4). The transition in the range of 10−30 °C accompanied by a magnitude loss of storage modulus can be assigned to the relaxation of the twists of the main chains. As shown in Figure 2c, the glass transition temperature (T_g) of P3HT with low molecular weight (i.e., P-9k) is relatively high, which is around 22 °C. P3HTs with molecular weight in the range of 15−21 kg/mol share a similar T_g. However, things are different when it comes to P-52k since there is a significant increase in the T_g value. The T_g of P3HT keeps increasing when the molecular weight is higher than 52 kg/mol. To some extent, our results are not completely consistent with what has been observed by Xie et al.[44] According to Xie's study, the T_g value of P3HT depends on the molecular weight and follows the Flory−Fox equation, and 14 kg/mol is the critical number-average molecular weight at which the tie chains between crystals form. From our results, we infer that P3HTs with low molecular weight are more likely to adopt an extended chain conformation and tend to transform from disordered aggregation to a highly ordered rod-like structure with a molecular weight increase, which results in the decrease of the thermal motion ability of the main chain. For P3HTs with a molecular weight higher than 15 kg/mol, the relaxation of the main chains occurs at lower temperatures, which is mainly due to the higher free volume provided by the increased length and flexibility of the polymer chains. The decreased motion ability of P-52k originates from the ordered packing of the polymer chains. In the meantime, the corresponding temperature of α transition increases from 15.7 °C for P-57k to 23.7 °C for P-74k, which is mainly due to the low mobility of the polymer chains resulting from the enhanced entanglement of P-74k.

2.4. Molecular Packing and Orientation Behaviors. To further confirm our inference, the GIWAXS measurement was

https://doi.org/10.1021/acsapm.1c01651
ACS Appl. Polym. Mater. 2022, 4, 1826−1835

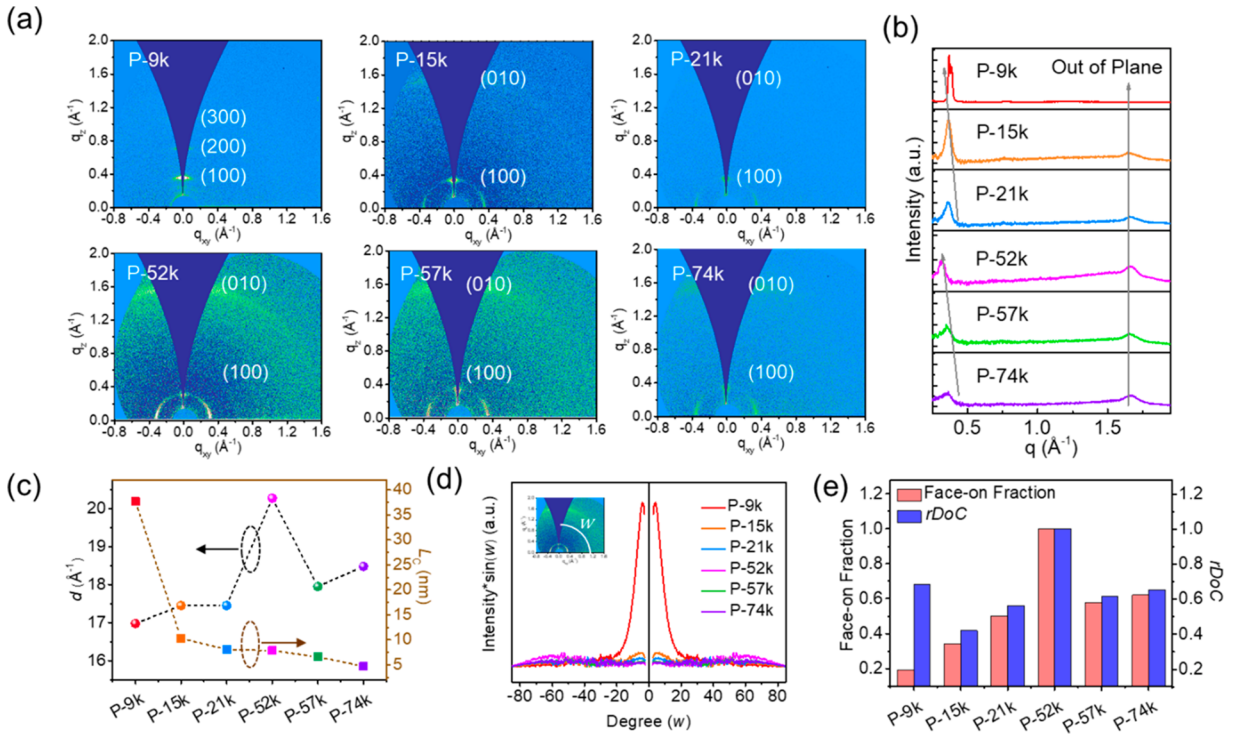

Figure 3. (a) GIWAXS patterns of six batches of P3HT polymers. (b) The OOP profiles extracted from their 2D patterns. (c) The plot of (100) d spacing and coherence length of P3HT samples along the OOP direction. (d) Pole figures extracted from the (100) diffraction along the OOP direction of the P3HT polymers. (e) Face-on fractions and rDoC values of the P3HT samples.

performed to investigate the crystalline texture and the degree of crystallinity of P3HTs with different molecular weights. The out-of-plane (OOP) profiles extracted from their 2D patterns (Figure 3a) are exhibited in Figure 3b. The obvious (100) diffraction pattern around 0.36 Å^{-1} along the OOP direction of all P3HT samples, assigned to the alkyl stacking, is indicative of the edge-on orientation relative to the substrate.[9] The (010) diffraction peak at 1.67 Å^{-1} in the OOP direction can be attributed to the $\pi-\pi$ stacking of P3HT. In addition, there are two weak peaks at 0.77 and 1.16 Å^{-1}, which belong to the (200) and (300) diffraction patterns, respectively.[45] It can be observed that P-9k only exhibits sharper and more intense lamellar stacking in the direction of OOP, while P3HTs with a molecular weight higher than 15 kg/mol display both obvious lamellar layer stacking and $\pi-\pi$ interchain stacking. Moreover, the intensities of the (200) and (300) diffraction peaks at 0.77 and 1.16 Å^{-1} decrease gradually with the molecular weight increasing from 15 to 74 kg/mol, indicating the molecular orientation of P3HT transforms from edge-on to a mixed manner composed of both edge-on and face-on orientation.

Table S3 summarized the crystallographic parameters of P3HTs with different molecular weights. As we can see from Figure 3c, the d_{100} value of P3HT is the lowest at the lowest molecular weight (i.e., 16.98 Å for P-9k), increases with a molecular weight increase, reaches the maximum (20.27 Å) in the intermediate molecular weight (i.e., 52 kg/mol), and subsequently decreases for P3HT with the higher molecular weight. This is consistent with what has been observed by Liu et al.; according to them, the reduction of the interlayer spacing of low molecular weight P3HT is mainly due to the disordered side-chain stacking in the solid state.[20] Previous studies[46,47] have demonstrated that P3HT with low molecular weight processes two different crystal polymorphs, namely, Form I and Form II; the difference between the two polymorphs is the side-chain conformation. Side chains in Form II, however, are more disordered, resulting in the reduced symmetry of the main-chain packing and layer spacing. Chlebosz et al.[46] pointed out that the increased interchain distance with larger molecular weight was mainly due to chain folding. Notably, P-9k has the strongest (100) diffraction intensity and the narrowest fwhm, corresponding to the high crystallinity and ordered structure. The fwhm increases from 0.055 Å^{-1} for P-15k to 0.12 Å^{-1} for P-74k, indicating the decreased ordering along the (100) direction with the molecular weight increase. All batches of P3HTs share a similar $\pi-\pi$ stacking distance except for P-9k. The $\pi-\pi$ coherence length of the polymers calculated from the Scherrer equation increases with a molecular weight increase and then decreases from 6.58 nm for P-52k to 4.83 nm for P-74k, which is indicative of the increased fraction of the disordered structure for the higher molecular weight P3HT. Compared with P-74k, P-57k has a longer $\pi-\pi$ coherence length, which in turn facilitates charge transport mobility.

The paracrystallinity disorder parameter[48] (g) used to describe the structure disorder in an imperfect crystal is calculated via the approximate formula:

$$g = \sqrt{\frac{1}{2\pi q}\Delta q} \tag{2}$$

where Δq is the fullwidth at half-maximum of the peak and q is the peak maximum of the (100) diffraction pattern. As displayed in Table S4, the g parameter keeps rising as the molecular weight increases from 9 to 74 kg/mol, indicating the increasing disorder fraction caused by the entanglement of the polymer chains. In order to provide a quantitative description of the effect of molecular weight on the crystallinity of P3HT,

https://doi.org/10.1021/acsapm.1c01651
ACS Appl. Polym. Mater. 2022, 4, 1826−1835

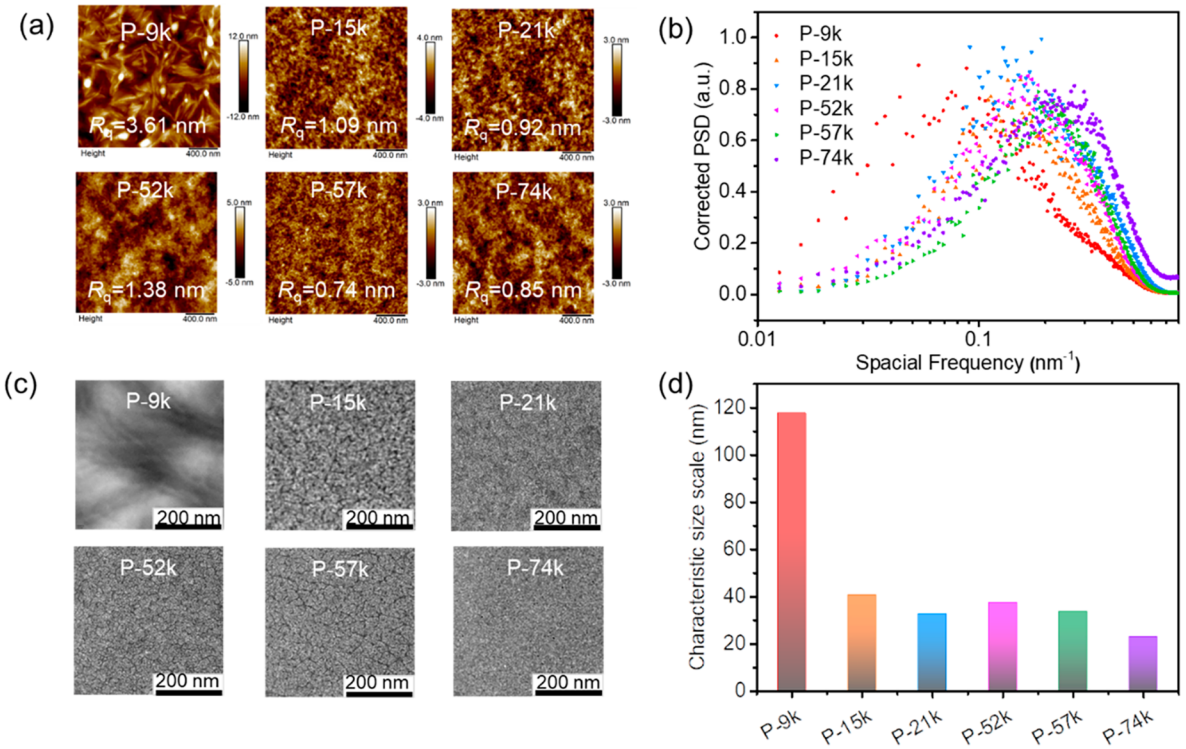

Figure 4. (a) AFM height images of the P3HT polymers. (b) PSD profiles extracted from the AFM phase images of P3HT. (c) TEM images of P3HT. (d) The characteristic size scale of P3HT.

the relative degree of crystallinity (rDoC)[49−51] is obtained by the approximate formula

$$\text{rDoC} \propto \int_{\omega_{\min}}^{\pi/2} I(\omega)\sin(\omega)\,\mathrm{d}(\omega) \tag{3}$$

rDoC is estimated by employing the pole figure (Figure 3d) of the (100) diffraction pattern, and ω and $I(\omega)$ are the polar angle and the scattered intensity along the polar angle, respectively. As shown in Figure 3e, the rDoC of P-9k is relatively high because of the formation of the grain boundaries between the crystalline domain. For P3HT with a molecular weight higher than 15 kg/mol, the rDoC increases to the maximum assigned to be 1.0 for P-52k, then decreases to 0.62 for P-57k, and finally levels off, which corresponds to the evolution of the degree of crystallinity and face-on fraction.

To further quantitatively analyze the orientation distribution of P3HT with different batches, the Hermans orientation parameter (S)[52] is calculated by the following formula:

$$S = \frac{1}{2}(3f_{\perp} - 1) \tag{4}$$

$$f_{\perp} = \frac{\int_0^{\pi/2} I(\omega)\cos^2(\omega)\sin(\omega)\,\mathrm{d}\omega}{\int_0^{\pi/2} I(\omega)\sin(\omega)\,\mathrm{d}\omega} \tag{5}$$

$f_{\perp}$ is the molecular orientation parameter and $I(\omega)$ is the total scattered intensity along the (100) peak at the corresponding polar angle. As exhibited in Table S4, P3HTs with a molecular weight lower than 9 kg/mol mainly adopt a preferential edge-on orientation, while higher molecular weight P3HTs generally display a face-on orientation. With the molecular weight increase, the S value of P3HT is more negative, indicating the more dominant face-on fraction. The maximum and minimum S values determined by P-9k and P-52k are 0.57 and −0.27, which correspond to the highest edge-on and face-on orientation percentages, respectively.

2.5. Morphology Properties. Tapping mode AFM was employed to investigate the influence of the molecular weight on the surface morphology of the P3HT films. The AFM height images of the P3HT films based on different molecular weights are displayed in Figure 4a. The root-mean-square surface roughness (R_q) of P3HT with a molecular weight lower than 15 kg/mol is relatively high, especially for P-9k, resulting from the formation of the grain boundaries between domains. P3HT with a molecular weight higher than 21 kg/mol except for P-52k possesses a similar R_q (∼1 nm), resulting in the formation of the comparable uniform morphology. It can be concluded that P3HT with a lower molecular weight obtains a higher degree of crystallinity, which agrees with the more intense (100) diffraction patterns along the OOP direction. Nevertheless, these crystals composed of chain ends and associated impurities are usually isolated and, therefore, limit charge transport, which is responsible for the relatively low hole mobility. In contrast, crystalline domains of higher molecular weight are connected by the longer polymer chains, which is favorable for the charge transport between crystalline domains.

Power spectral density (PSD) profiles (Figure 4b) extracted from the AFM phase images were plotted to quantitatively compare the phase-separated morphology of P3HT with different batches. As depicted in Figure 4d, P3HT with sufficiently low molecular weight (i.e., P-9k) processes the largest domain spacing of ∼118 nm because of the high concentration of grain boundaries. P3HT with a molecular weight higher than 15 kg/mol, except for that of P-74k, exhibits a similar domain spacing, indicating that the surface morphology and phase separation of P3HT films are not much

https://doi.org/10.1021/acsapm.1c01651
ACS Appl. Polym. Mater. 2022, 4, 1826−1835

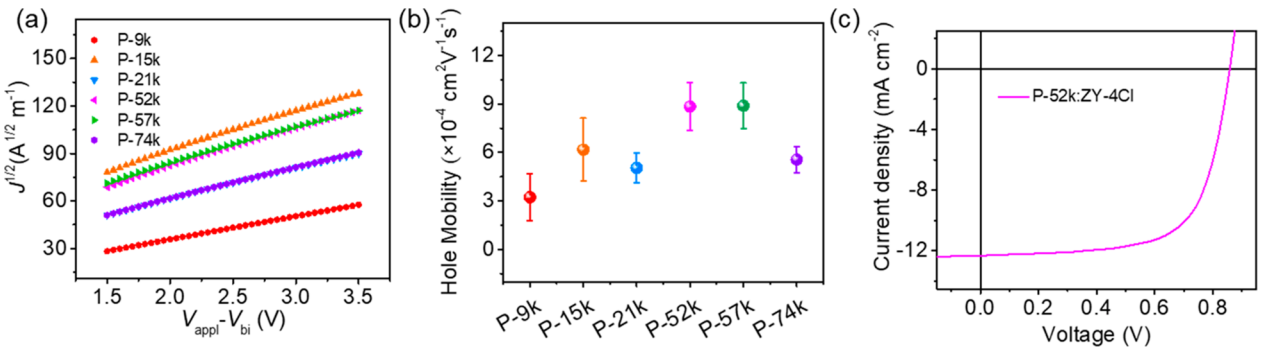

Figure 5. (a) Plots of $J_{1/2}$ versus $V_{eff} - V_{bi}$. (b) Hole mobilities of various P3HT batches in single charge carrier diodes. (c) The typical $J-V$ curve of P3HT:ZY-4Cl-based photovoltaic devices.

different. These observations also can be supported by the TEM images (Figure 4c). It can be clearly seen that P3HT with a molecular weight higher than 15 kg/mol exhibits a more uniform morphology and more obvious nanoscaled interpenetrating network structure. Nevertheless, P-74k does not follow this tendency; the dark dots in the TEM image can be ascribed to the P3HT aggregation, which is mainly due to the limited solubility of the higher molecular weight P3HT in THF.

2.6. Electrical Properties. The space charge limited current (SCLC) method is used to investigate the charge carrier mobility (ITO/PEDOT:PSS/P3HT/MoO_3/Al) of P3HT (Figure 5a) with different batches. The hole mobility as a function of molecular weight is displayed in Figure 5b, and the corresponding parameters are summarized in Table S2. The hole mobility of P3HT first increases to the maximum and then levels off with molecular weight increasing from 9 to 57 kg/mol followed by the decreases from $(8.89 \pm 1.41) \times 10^{-4}$ $cm^2V^{-1}s^{-1}$ for P-57k to $(5.65 \pm 0.82) \times 10^{-4}$ $cm^2V^{-1}s^{-1}$ for P-74k. The reduced hole mobility for P3HT with a low molecular weight is mainly due to the grain boundaries formed between the highly ordered crystalline restricting interchain charge transport, while the crystalline domains connected by the long polymer chains of higher molecular weight P3HT provide continuous charge transport pathways contributing to the intrachain charge transport, which is much faster than interchain transport. P-74k with a comparable number-average molecular weight to P-57k obtains lower hole mobility. The possible reason is that the randomly packed longer polymer chains of highly polydisperse P3HT suppress the ordered alignment of P3HT, which deteriorates the charge transport mobility of P-74k.

Considering the relatively low open-circuit voltage of P3HT-based organic photovoltaic cells, the introduction of nonfullerene acceptors matched well with P3HT is an effective method to realize a higher V_{oc} and PCE.[53,54] Photovoltaic devices based on the highest mobility P3HT batch (P-52k) and a recently developed nonfullerene acceptor, namely, ZY-4Cl,[32] were fabricated to further evaluate the photovoltaic performance of the DArP prepared P3HT in nonfullerene organic solar cells. As shown in Figure 5c, the blend system achieves a decent PCE of 7.10%, which suggests that the DArP prepared P3HTs are promising materials for low-cost organic solar cells. We note that the PCE is somehow lower than that of the conventionally synthesized P3HT used in Hou and coworkers' work.[32] A close inspection of the two studies reveals that the molecular weight and PDI of P-52k used in this work are comparable to those in Hou and coworkers' work. Nevertheless, the regioregularity of P3HT also plays a critical role in the electrical performance of the blend system. Compared to the regioregularity (91% ∼ 94%) in Hou and coworkers' work, the regioregularity (∼89%) of P-52k is slightly lower. Thus, P-52k used in this work contains more HH and TT defects, which suppress the effective transport of the charge carrier and thus result in the lower PCE. Crucially, a comparative study of the physical properties and electrical performance of the DArP prepared P3HT and conventionally synthesized P3HT is an important research area, which requires the synergistic control of all three structural parameters (molecular weight, PDI, and regioregularity). Such a comparative study, however, requires extensive synthetic explorations and thus is beyond the scope of our study, which focuses exclusively on revealing the properties of P3HT prepared via DArP.

3. CONCLUSION

In summary, we successfully synthesized a series of P3HT by DArP and systematically investigated their physical properties as a function of molecular weight to reveal the correlation between molecular structure parameters and electronic device performance. It turns out that hole mobility does not monotonously increase with a molecular weight increase but reaches a maximum at the intermediate molecular weight (∼50 kg/mol) at which both the degrees of aggregation and crystallinity are the highest. Despite the relatively high crystallization tendency for P3HT with a low molecular weight, the hole mobility lags behind that of higher molecular weight ones as a result of the formation of unconnected grain boundaries. With the increase of molecular weight, P3HT polymer chains transform from lamellar preferential stacking to $\pi-\pi$ dominated orientation, contributing to the increase of interchain charge transport. On the other hand, the crystalline domains are connected by long polymer chains, which provide interconnected pathways for intrachain charge transport. The hole mobility of P3HT begins to saturate when molecular weight further increases due to the increase of disordered content resulting from the enhanced entanglement. Moreover, the photovoltaic devices based on a Y6-series nonfullerene acceptor and the best P3HT batch revealed in this study (i.e., P-52k) achieve a presentable PCE of over 7%. We hope this study can provide some insights into the physical properties of P3HT and related low-cost materials made via eco-friendly polycondensation protocols.

https://doi.org/10.1021/acsapm.1c01651
ACS Appl. Polym. Mater. 2022, 4, 1826−1835

4. EXPERIMENTAL SECTION

4.1. Physical Properties and Morphology Characterizations. The UV−vis absorption spectra of all batches of P3HT in solutions (THF) and in the solid state (by spin-coating their solution on the quartz substrates) were carried out using a Shimadzu UV-3600 Plus spectrometer. DSC was employed to investigate the thermal properties of P3HT. P3HT with different molecular weights were dissolved in THF with a concentration of 15 mg/mL, drop-cast on clean glass slides, and then dried in a vacuum overnight to remove the residual solvent followed by the transformation to the DSC pan. The DSC data were all acquired on a TA Q25 DSC under a nitrogen atmosphere with a cooling/heating rate of 10 °C/min. DMA measurements were performed on a TA Q800 DMA. P3HT solutions (15 mg/mL) were carefully drop-coated on glass fiber to guarantee the uniform coverage of samples and dried in high vacuum for 8 h. The DMA characterizations were carried out in strain-controlled mode at the frequency of 1 Hz with a heating rate of 3 °C/min.

GIWAXS measurements were performed in the beamline BL14B1 of Shanghai Synchrotron Radiation Facility (SSRF) beamline. Part of the sample characterizations were carried out on the beamline BL02U2. The P3HT films with different molecular weights were deposited over the silicon substrates with the conditions similar to the ones used for device fabrication. All the samples were irradiated at a fixed incident angle of 0.2° for the complete penetration of the X-ray. The beam center and sample-to-detector distance were calibrated with LaB_6, and the X-ray wavelength was 0.168 nm. The nanoscale surface morphology of different batches of P3HT was detected by an AFM instrument (Bruker Multimode 8) in tapping mode. TEM images were captured by a JEM-2100PLUS electron microscope (JEOL) at an accelerating voltage of 120 kV. The thickness of the P3HT thin films was measured by the surface profilometer Bruker Dektak XT.

4.2. Device Fabrication and Characterization. The space charge limited current (SCLC) devices in the configurations of ITO/PEDOT:PSS/P3HT/MoO_3/Al were prepared to investigate the charge carrier mobility of different batches of P3HT. The hole mobilities were calculated by the equation:

$$J = \left(\frac{9}{8}\right)\varepsilon_0\varepsilon\mu_0 V^2/L^3 \exp(0.89\sqrt{V/E_0 L}) \quad (6)$$

where J is the current density, ε_0 is the permittivity of the vacuum, ε is the relative permittivity of the material, μ_0 is the zero field hole mobility, V is the effective applied voltage, and L is the thickness of the film. The ITO substrates were cleaned ultrasonically with detergent, deionized water, acetone, and isopropanol for 15 min, respectively, dried by nitrogen flow, and then treated with ultraviolet−ozone for 25 min. The PEDOT:PSS solution filtered through a 0.45 μm filter was spin-coated on the ITO substrates at 4000 rpm for 40 s and annealed at 150 °C for 20 min. The thickness of the PEDOT:PSS film was about 30 nm. Different batches of P3HT dissolved in THF (15 mg/mL) were spin-coated onto the PEDOT:PSS layers at 1500 rpm for 40 s followed by thermal annealing at 130 °C for 10 min. Finally, the 6 nm-thick MoO_3 and 100 nm-thick Al were deposited on the top of the P3HT surface under the pressure of 1.5×10^{-4} Pa. The conventional device of ITO/PEDOT:PSS/P3HT:ZY-4Cl/PDINO/Al was fabricated by employing the same deposition condition of the SCLC devices, except that the ∼10 nm-thick PDINO was spin-coated on the top of the active layer at 3000 rpm for 40 s, and the effective working area of the photovoltaic devices was about 0.04 cm^2. The J−V curves of P3HT with different molecular weights were measured by a Keithley 2400 source meter under AM1.5G irradiation with an intensity of 100 mW/cm^2.

■ ASSOCIATED CONTENT

Supporting Information

The Supporting Information is available free of charge at https://pubs.acs.org/doi/10.1021/acsapm.1c01651.

NMR data of DArP prepared P3HT polymers; UV−vis absorption spectra of DArP prepared P3HT polymers; DMA data of DArP prepared P3HT polymers; GIWAXS data analysis of DArP prepared P3HT polymers (PDF)

■ AUTHOR INFORMATION

Corresponding Authors

Long Ye − *School of Materials Science and Engineering, Tianjin Key Laboratory of Molecular Optoelectronic Sciences, Tianjin University, Tianjin 300350, China; State Key Laboratory of Applied Optics, Changchun Institute of Optics, Fine Mechanics and Physics, Chinese Academy of Sciences, Changchun 130033, China;* orcid.org/0000-0002-5884-0083; Email: yelong@tju.edu.cn

Huizhen Ke − *Fujian Key Laboratory of Novel Functional Textile Fibers and Materials, Minjiang University, Fuzhou 350108, China; Fujian Key Laboratory of Electrochemical Energy Storage Materials, Fuzhou University, Fuzhou 350108, China*; Email: kehuizhen2013@163.com

Authors

Qingchun Qi − *School of Materials Science and Engineering, Tianjin Key Laboratory of Molecular Optoelectronic Sciences, Tianjin University, Tianjin 300350, China; State Key Laboratory of Applied Optics, Changchun Institute of Optics, Fine Mechanics and Physics, Chinese Academy of Sciences, Changchun 130033, China*

Yuan Zhong − *School of Materials Science and Engineering, Tianjin Key Laboratory of Molecular Optoelectronic Sciences, Tianjin University, Tianjin 300350, China*

Yang Liu − *School of Materials Science and Engineering, Tianjin Key Laboratory of Molecular Optoelectronic Sciences, Tianjin University, Tianjin 300350, China*

Mengyuan Gao − *School of Materials Science and Engineering, Tianjin Key Laboratory of Molecular Optoelectronic Sciences, Tianjin University, Tianjin 300350, China;* orcid.org/0000-0001-9446-2879

Zhongxiang Peng − *School of Materials Science and Engineering, Tianjin Key Laboratory of Molecular Optoelectronic Sciences, Tianjin University, Tianjin 300350, China*

Saimeng Li − *School of Materials Science and Engineering, Tianjin Key Laboratory of Molecular Optoelectronic Sciences, Tianjin University, Tianjin 300350, China*

Wenchao Zhao − *Co-Innovation Center of Efficient Processing and Utilization of Forest Resources, College of Materials Science and Engineering, Nanjing Forestry University, Nanjing 210037, China;* orcid.org/0000-0001-8717-1774

Jidong Zhang − *State Key Laboratory of Polymer Physics and Chemistry, Changchun Institute of Applied Chemistry, Chinese Academy of Sciences, Changchun 130022, China*

Complete contact information is available at: https://pubs.acs.org/10.1021/acsapm.1c01651

Author Contributions

The manuscript was written through the contributions of all authors. All authors have given approval to the final version of the manuscript.

Notes

The authors declare no competing financial interest.

https://doi.org/10.1021/acsapm.1c01651
ACS Appl. Polym. Mater. 2022, 4, 1826−1835

■ ACKNOWLEDGMENTS

We are grateful for the financial support from the National Science Foundation of China (No. 52073207), the Open Fund of State Key Laboratory of Applied Optics (No. SKLAO2021001A17), the Open Fund of Fujian Key Laboratory of Electrochemcial Energy Storage Materials, Fuzhou University (NO. 2021CN02), and the start-up grant of Peiyang Scholar program from Tianjin University. The beamline BL14B1 and beamline BL02U2 of Shanghai Synchrotron Radiation Facility are appreciated for supporting the two-dimensional GIWAXS measurement. The authors greatly acknowledge Prof. Yanhou Geng for stimulating discussions and providing the synthetic chemistry facility.

■ REFERENCES

(1) Kleinschmidt, A. T.; Root, S. E.; Lipomi, D. J. Poly(3-hexylthiophene) (P3HT): Fruit Fly or Outlier in Organic Solar Cell Research? *J. Mater. Chem. A* **2017**, *5*, 11396−11400.

(2) Ashraf, R. S.; Meager, I.; Nikolka, M.; Kirkus, M.; Planells, M.; Schroeder, B. C.; Holliday, S.; Hurhangee, M.; Nielsen, C. B.; Sirringhaus, H.; McCulloch, I. Chalcogenophene Comonomer Comparison in Small Band Gap Diketopyrrolopyrrole-Based Conjugated Polymers for High-Performing Field-Effect Transistors and Organic Solar Cells. *J. Am. Chem. Soc.* **2015**, *137*, 1314−1321.

(3) Nikolka, M.; Nasrallah, I.; Rose, B.; Ravva, M. K.; Broch, K.; Sadhanala, A.; Harkin, D.; Charmet, J.; Hurhangee, M.; Brown, A.; Illig, S.; Too, P.; Jongman, J.; McCulloch, I.; Bredas, J. L.; Sirringhaus, H. High Operational and Environmental Stability of High-Mobility Conjugated Polymer Field-Effect Transistors Through the Use of Molecular Additives. *Nat. Mater.* **2017**, *16*, 356−363.

(4) Quinn, J. T. E.; Zhu, J. X.; Li, X.; Wang, J. L.; Li, Y. N. Recent Progress in the Development of n-Type Organic Semiconductors for Organic Field Effect Transistors. *J. Mater. Chem. C* **2017**, *5*, 8654−8681.

(5) Yang, J.; Zhao, Z. Y.; Wang, S.; Guo, Y. L.; Liu, Y. Q. Insight into High-Performance Conjugated Polymers for Organic Field-Effect Transistors. *Chem.* **2018**, *4*, 2748−2785.

(6) Fuentes-Hernandez, C.; Chou, W.-F.; Khan, T. M.; Diniz, L.; Lukens, J.; Larrain, F. A.; Rodriguez-Toro, V. A.; Kippelen, B. Large-Area Low-Noise Flexible Organic Photodiodes for Detecting Faint Visible Light. *Science* **2020**, *370*, 698.

(7) H., V.; S. P., A.; L., Y.; M., N.; M., V.; H., D. Flexible and high energy density solid-state asymmetric supercapacitor based on polythiophene nanocomposites and charcoal. *RSC Adv.* **2018**, *8*, 31414−31426.

(8) Kaminorz, Y.; Smela, E.; Johansson, T.; Brehmer, L.; Andersson, M. R.; Inganas, O.; et al. Characteristics of polythiophene surface light emitting diodes. *Synth. Met.* **2000**, *113*, 103−114.

(9) Pei, J.; Yu, W. L.; Huang, W.; Heeger, A. J. A novel series of efficient thiophene-based light-emitting conjugated polymers and application in polymer light-emitting diodes. *Macromolecules* **2000**, *33*, 2462−2471.

(10) Perepichka, I. F.; Perepichka, D. F.; Meng, H.; Wudl, F. Light-Emitting Polythiophenes. *Adv. Mater.* **2005**, *17*, 2281−2305.

(11) Wu, Y.; Bai, H.; Wang, Z.; Cheng, P.; Zhu, S.; Wang, Y.; Ma, W.; Zhan, X. A Planar Electron Acceptor for Efficient Polymer Solar Cells. *Energy Environ. Sci.* **2015**, *8*, 3215−3221.

(12) Xu, X.; Zhang, G.; Yu, L.; Li, R.; Peng, Q. P3HT-Based Polymer Solar Cells with 8.25% Efficiency Enabled by a Matched Molecular Acceptor and Smart Green-Solvent Processing Technology. *Adv. Mater.* **2019**, *31*, 1906045.

(13) Li, S.; Liu, W.; Shi, M.; Mai, J.; Lau, T.-K.; Wan, J.; Lu, X.; Li, C.-Z.; Chen, H. A spirobifluorene and diketopyrrolopyrrole moieties based non-fullerene acceptor for efficient and thermally stable polymer solar cells with high open-circuit voltage. *Energy Environ. Sci.* **2016**, *9*, 604−610.

(14) Liang, Q.; Jiao, X.; Yan, Y.; Xie, Z.; Lu, G.; Liu, J.; Han, Y. Separating Crystallization Process of P3HT and O-IDTBR to Construct Highly Crystalline Interpenetrating Network with Optimized Vertical Phase Separation. *Adv. Funct. Mater.* **2019**, *29*, 1807591.

(15) Wang, Q.; Li, M.; Peng, Z.; Kirby, N.; Deng, Y.; Ye, L.; Geng, Y. Calculation Aided Miscibility Manipulation Enables Highly Efficient Polythiophene:Nonfullerene Photovoltaic Cells. *Sci. China Chem.* **2021**, *64*, 478−487.

(16) Bruner, C.; Dauskardt, R. Role of Molecular Weight on the Mechanical Device Properties of Organic Polymer Solar Cells. *Macromolecules* **2014**, *47*, 1117−1121.

(17) Dang, M. T.; Hirsch, L.; Wantz, G.; Wuest, J. D. Controlling the Morphology and Performance of Bulk Heterojunctions in Solar Cells. Lessons Learned From the Benchmark Poly(3-hexylthiophene): [6,6]-phenyl-C61-butyric Acid Methyl Ester System. *Chem. Rev.* **2013**, *113*, 3734−3765.

(18) Katsouras, A.; Gasparini, N.; Koulogiannis, C.; Spanos, M.; Ameri, T.; Brabec, C. J.; Chochos, C. L.; Avgeropoulos, A. Systematic Analysis of Polymer Molecular Weight Influence on the Organic Photovoltaic Performance. *Macromol. Rapid Commun.* **2015**, *36*, 1778−1797.

(19) Koch, F. P. V.; Rivnay, J.; Foster, S.; Müller, C.; Downing, J. M.; Buchaca-Domingo, E.; Westacott, P.; Yu, L.; Yuan, M.; Baklar, M.; Fei, Z.; Luscombe, C.; McLachlan, M. A.; Heeney, M.; Rumbles, G.; Silva, C.; Salleo, A.; Nelson, J.; Smith, P.; Stingelin, N. The Impact of Molecular Weight on Microstructure and Charge Transport in Semicrystalline Polymer Semiconductors−Poly(3-hexylthiophene), A Model Study. *Prog. Polym. Sci.* **2013**, *38*, 1978−1989.

(20) Liu, F.; Chen, D.; Wang, C.; Luo, K.; Gu, W.; Briseno, A. L.; Hsu, J. W.; Russell, T. P. Molecular Weight Dependence of the Morphology in P3HT:PCBM Solar Cells. *ACS Appl. Mater. Interfaces* **2014**, *6*, 19876−19887.

(21) Ma, W.; Kim, J. Y.; Lee, K.; Heeger, A. J. Effect of the Molecular Weight of Poly(3-hexylthiophene) on the Morphology and Performance of Polymer Bulk Heterojunction Solar Cells. *Macromol. Rapid Commun.* **2007**, *28*, 1776−1780.

(22) Paquin, F.; Yamagata, H.; Hestand, N. J.; Sakowicz, M.; Berube, N.; Cote, M.; Reynolds, L. X.; Haque, S. A.; Stingelin, N.; Spano, F. C.; Silva, C. Two-Dimensional Spatial Coherence of Excitons in Semicrystalline Polymeric Semiconductors: Effect of Molecular Weight. *Phys. Rev. B* **2013**, *88*, 155202.

(23) Kline, R. J.; McGehee, M. D.; Kadnikova, E. N.; Liu, J. S.; Frechet, J. M. J.; Toney, M. F. Dependence of Regioregular Poly(3-hexylthiophene) Film Morphology and Field-Effect Mobility on Molecular Weight. *Macromolecules* **2005**, *38*, 3312−3319.

(24) Marrocchi, A.; Lanari, D.; Facchetti, A.; Vaccaro, L. Poly(3-hexylthiophene): Synthetic Methodologies and Properties in Bulk Heterojunction Solar Cells. *Energy Environ. Sci.* **2012**, *5*, 8457−8474.

(25) McCullough, R. D.; Lowe, R. D. Enhanced Electrical Conductivity in Regioselectively Synthesized Poly(3-al kylthiophenes). *J. Chem. Soc., Chem. Commun.* **1992**, *1*, 70−72.

(26) Sun, M. M.; Zhou, M. L.; Liang, L. Y.; Wang, W.; Wang, W.; Ling, Q. D. Research Progress in Conjugated Polymer Prepared by Direct (hetero) arylation Polycondensation. *Macromol. Rapid Commun.* **2013**, *33*, 2504−2514.

(27) Sevignon, M.; Papillon, J.; Schulz, E.; Lemaire, M. New Synthetic Method for the Polymerization of Alkylthiophenes. *Tetrahedron Lett.* **1999**, *40*, 5873−5876.

(28) Wang, Q. F.; Takita, R.; Kikuzaki, Y.; Ozawa, F. Palladium-Catalyzed Dehydrohalogenative Polycondensation of 2-Bromo-3-hexylthiophene: An Efficient Approach to Head-to-Tail Poly(3-hexylthiophene). *J. Am. Chem. Soc.* **2010**, *132*, 11420−11421.

(29) Mainville, M.; Leclerc, M. Direct (hetero)arylation: A Tool for Low-Cost and Eco-friendly Organic Photovoltaics. *ACS Appl. Polym. Mater.* **2021**, *3*, 2−13.

(30) Liu, Y.; Xian, K. H.; Peng, Z. X.; Gao, M. Y.; Shi, Y. B.; Deng, Y. F.; Geng, Y. H.; Ye, L. Tuning the Molar Mass of P3HT via Direct Arylation Polycondensation Yields Optimal Interaction and High

https://doi.org/10.1021/acsapm.1c01651
ACS Appl. Polym. Mater. 2022, 4, 1826−1835

Efficiency in Nonfullerene Organic Solar Cells. *J. Mater. Chem. A* **2021**, *9*, 19874−19885.
(31) Liu, Y.; Xian, K. H.; Gui, R. H.; Zhou, K. K.; Liu, J. W.; Gao, M. Y.; Zhao, W. C.; Jiao, X. C.; Deng, Y. F.; Yin, H.; Ye, L. Simple Polythiophene Solar Cells Approaching 10% Efficiency via Carbon-Chain Length Modulation of Poly(3-alkylthiophene). *Macromolecules* **2022**, *55*, 133−145.
(32) Yang, C.; Zhang, S.; Ren, J.; Gao, M.; Bi, P.; Ye, L.; Hou, J. Molecular Design of a Non-Fullerene Acceptor Enables a P3HT-Based Organic Solar Cell with 9.46% Efficiency. *Energy Environ. Sci.* **2020**, *13*, 2864−2869.
(33) Adachi, T.; Brazard, J.; Ono, R. J.; Hanson, B.; Traub, M. C.; Wu, Z.-Q.; Li, Z.; Bolinger, J. C.; Ganesan, V.; Bielawski, C. W.; Vanden Bout, D. A.; Barbara, P. F. Regioregularity and Single Polythiophene Chain Conformation. *J. Phys. Chem. Lett.* **2011**, *2*, 1400−1404.
(34) Custódio Mota, I.; Pedroso Silva Santos, B.; Értola Pereira dos Santos, R.; Banar Guedes, L.; Tenório Soares, I.; Rubio Arias, J. J.; Lopes de Araújo, F.; Nogueira, A. F.; Vieira Marques, M. d. F. Influence of Reaction Time on Properties of Regioregular Poly(3-hexylthiophene) by the Grignard Metathesis Polymerization. *J. Therm. Anal. Calorim.* **2021**, DOI: 10.1007/s10973-021-10890-4.
(35) Zen, A.; Saphiannikova, M.; Neher, D.; Grenzer, J.; Grigorian, S.; Pietsch, U.; Asawapirom, U.; Janietz, S.; Scherf, U.; Lieberwirth, I.; Wegner, G. Effect of Molecular Weight on the Structure and Crystallinity of Poly(3-hexylthiophene). *Macromolecules* **2006**, *39*, 2162−2171.
(36) Trznadel, M.; Pron, A.; Zagorska, M. Effect of Molecular Weight on Spectroscopic and Spectroelectrochemical Properties of Regioregular Poly(3-hexylthiophene). *Macromolecules* **1998**, *31*, 5051−5058.
(37) Clark, J.; Silva, C.; Friend, R. H.; Spano, F. C. Role of Intermolecular Coupling in the Photophysics of Disordered Organic Semiconductors: Aggregate Emission in Regioregular Polythiophene. *Phys. Rev. Lett.* **2007**, *98*, 206406.
(38) Clark, J.; Chang, J. F.; Spano, F. C.; Friend, R. H.; Silva, C. Determining Exciton Bandwidth and Film Microstructure in Polythiophene Films Using Linear Absorption Spectroscopy. *Appl. Phys. Lett.* **2009**, *94*, 163306.
(39) Chang, J.-F.; Clark, J.; Zhao, N.; Sirringhaus, H.; Breiby, D. W.; Andreasen, J. W.; Nielsen, M. M.; Giles, M.; Heeney, M.; McCulloch, I. Molecular-Weight Dependence of Interchain Polaron Delocalization and Exciton Bandwidth in High-Mobility Conjugated Polymers. *Phys. Rev. B* **2006**, *74*, 115318.
(40) Liu, J.; Arif, M.; Zou, J.; Khondaker, S. I.; Zhai, L. Controlling Poly(3-hexylthiophene) Crystal Dimension: Nanowhiskers and Nanoribbons. *Macromolecules* **2009**, *42*, 9390−9393.
(41) Chandrasekaran, N.; Kumar, A.; Thomsen, L.; Kabra, D.; McNeill, C. R. High Performance As-Cast P3HT:PCBM Devices: Understanding the Role of Molecular Weight in High Regioregularity P3HT. *Mater. Adv.* **2021**, *2*, 2045−2054.
(42) Remy, R.; Weiss, E. D.; Nguyen, N. A.; Wei, S. J.; Campos, L. M.; Kowalewski, T.; Mackay, M. E. Enthalpy of Fusion of Poly(3-hexylthiophene) by Differential Scanning Calorimetry. *J. Polym. Sci. B Polym. Phys.* **2014**, *52*, 1469−1475.
(43) Wu, Z.; Petzold, A.; Henze, T.; Thurn-Albrecht, T.; Lohwasser, R. H.; Sommer, M.; Thelakkat, M. Temperature and Molecular Weight Dependent Hierarchical Equilibrium Structures in Semiconducting Poly(3-hexylthiophene). *Macromolecules* **2010**, *43*, 4646−4653.
(44) Xie, R.; Lee, Y.; Aplan, M. P.; Caggiano, N. J.; Müller, C.; Colby, R. H.; Gomez, E. D. Glass Transition Temperature of Conjugated Polymers by Oscillatory Shear Rheometry. *Macromolecules* **2017**, *50*, 5146−5154.
(45) Xian, K.; Liu, Y.; Liu, J.; Yu, J.; Xing, Y.; Peng, Z.; Zhou, K.; Gao, M.; Zhao, W.; Lu, G.; Zhang, J.; Hou, J.; Geng, Y.; Ye, L. Delicate crystallinity control enables high-efficiency P3HT organic photovoltaic cells. *J. Mater. Chem. A* **2022**, *10*, 3418−3429.
(46) Chlebosz, D.; Janasz, L.; Pisula, W.; Kiersnowski, A. Relationship Between Crystalline Structure of Poly(3-hexylthiophene) Blends and Properties of Organic Thin-Film Transistors − A Brief Review. *Polymer* **2016**, *61*, 433−441.
(47) Rivnay, J.; Mannsfeld, S. C.; Miller, C. E.; Salleo, A.; Toney, M. F. Quantitative Determination of Organic Semiconductor Microstructure from the Molecular to Device Scale. *Chem. Rev.* **2012**, *112*, 5488−5519.
(48) Pei, D.; Wang, Z.; Peng, Z.; Zhang, J.; Deng, Y.; Han, Y.; Ye, L.; Geng, Y. Impact of Molecular Weight on the Mechanical and Electrical Properties of a High-Mobility Diketopyrrolopyrrole-Based Conjugated Polymer. *Macromolecules* **2020**, *53*, 4490−4500.
(49) Boudouris, B. W.; Ho, V.; Jimison, L. H.; Toney, M. F.; Salleo, A.; Segalman, R. A. Real-Time Observation of Poly(3-alkylthiophene) Crystallization and Correlation with Transient Optoelectronic Properties. *Macromolecules* **2011**, *44*, 6653−6658.
(50) Peng, Z.; Jiang, K.; Qin, Y.; Li, M.; Balar, N.; O'Connor, B. T.; Ade, H.; Ye, L.; Geng, Y. Modulation of Morphological, Mechanical, and Photovoltaic Properties of Ternary Organic Photovoltaic Blends for Optimum Operation. *Adv. Energy Mater.* **2021**, *11*, 2003506.
(51) Peng, Z.; Ye, L.; Ade, H. Understanding, quantifying, and controlling the molecular ordering of semiconducting polymers: from novices to experts and amorphous to perfect crystals. *Mater. Horiz.* **2022**, *9*, 577.
(52) Perez, L. A.; Zalar, P.; Ying, L.; Schmidt, K.; Toney, M. F.; Nguyen, T.-Q.; Bazan, G. C.; Kramer, E. J. Effect of Backbone Regioregularity on the Structure and Orientation of a Donor−Acceptor Semiconducting Copolymer. *Macromolecules* **2014**, *47*, 1403−1410.
(53) Xiao, B.; Tang, A.; Zhang, J.; Mahmood, A.; Wei, Z.; Zhou, E. Achievement of High Voc of 1.02 V for P3HT-Based Organic Solar Cell Using a Benzotriazole-Containing Non-Fullerene Acceptor. *Adv. Energy Mater.* **2017**, *7*, 1602269.
(54) Xiao, B.; Tang, A.; Yang, J.; Wei, Z.; Zhou, E. P3HT-Based Photovoltaic Cells with a High Voc of 1.22 V by Using a Benzotriazole-Containing Nonfullerene Acceptor End-Capped with Thiazolidine-2,4-dione. *ACS Macro Lett.* **2017**, *6*, 410−414.